Istraživanja i projektovanja za privredu
ISSN 1451-4117
DOI:10.5937/jaes0-65371
www.engineeringscience.rs

iipp publishing

Journal of Applied Engineering Science
Review Paper,
Volume 24, Number 3, Year 2026,
no 1352, pp 542-554

EFFECT OF PREHEATING TEMPERATURE ON THE MECHANICAL PROPERTIES AND MICROSTRUCTURAL EVOLUTION OF SMAW-WELDED ASTM A36 STEEL

Sumarji Marji[1], Agus Suprihanto[1], Arif Wahyudiyanto[2], Agus Hariyanto[3]*, Wajilan[3]

[1]Diponegoro University, Faculty of Engineering, Department of Mechanical Engineering, Semarang, Indonesia
[2]Semarang State Polytechnic, Mechanical Engineering, Department of Mechanical Engineering, Semarang, Indonesia
[3]Samarinda State Polytechnic, Mechanical Engineering, Department of Mechanical Engineering, Samarinda, Indonesia

**agus.hariyanto@polnes.ac.id*

This study examines the effect of preheating temperature (N/A, 150 °C, 250 °C, and 350 °C) on the mechanical performance and microstructural evolution of SMAW-welded ASTM A36 steel. Welding was performed under controlled conditions using E7016 and E7018 electrodes, and joint properties were evaluated through tensile testing, Vickers hardness profiling, and metallographic analysis in the WM, HAZ, and BM regions. The ultimate tensile strength remained relatively stable (443–446 MPa), whereas yield strength and ductility varied with preheating temperature. The 250 °C condition yielded the highest yield strength (315.68 MPa) and the most uniform hardness distribution, indicating moderated cooling behaviour. Microstructural analysis revealed a refinement–stabilisation–coarsening trend with increasing preheat, with 250 °C producing the most homogeneous ferrite–pearlite structure, while 350 °C promoted grain coarsening and softening.

Keywords: ASTM A36 steel, SMAW, preheating temperature, heat-affected zone (HAZ), microstructural evolution

HIGHLIGHTS

- Preheating temperature strongly influences microstructure evolution in SMAW-welded ASTM A36 steel.
- Preheating at 250 °C produces the highest yield strength and most uniform hardness profile.
- Microstructure changes from refined to coarser grains with increasing preheating temperature.
- Excessive preheating at 350 °C promotes grain growth and softening in the HAZ

1 Introduction

ASTM A36 steel is a low-carbon structural steel widely used in welded structural applications because of its favourable mechanical properties and weldability. It is broadly comparable, but not directly equivalent, to S235JR steel for general structural applications. Despite good weldability, weld cracking is affected by carbon equivalent, hydrogen, cooling rate, heat input, and restraint [1]. Welding thermal cycles alter the microstructure, mechanical response, and residual stress across the WM, HAZ, and BM [2, 3, 4].

SMAW has been applied to ASTM A36 steel for stainless-steel cladding and butt- and lap-joint welding applications [5, 6]. The resulting welded joints have been evaluated in terms of tensile behaviour, hardness, microstructural characteristics, and residual-stress development [3–6]. In SMAW-welded ASTM A36 steel, electrode type and welding parameters affect joint properties [7]. Rapid cooling can increase hardness, retain diffusible hydrogen, and raise crack susceptibility, particularly under high restraint [1, 8].

Preheating is commonly employed in steel welding to reduce temperature gradients and control cooling rates in the weld region [9, 10]. Where diffusible hydrogen and crack-susceptible microstructures are present, reducing cooling severity can help minimise the risk of hydrogen-assisted cracking [1]. By increasing the initial base-metal temperature, preheating reduces the cooling rate and promotes a more controlled welding thermal cycle, thereby influencing the microstructure and mechanical response of the joint [11, 12]. Previous studies reported that increasing preheating can reduce cooling-induced martensitic transformation and local microhardness in laser-welded AH36 steel, while appropriate preheating in arc-welded mild steel can improve microstructural homogeneity, tensile strength, and ductility [12, 13].

Changes in welding thermal conditions can modify the microstructures of the weld metal (WM) and heat-affected zone (HAZ), thereby influencing localized hardness and tensile behaviour of welded joints [14, 15]. Tensile testing evaluates UTS, YS, and elongation, whereas Vickers hardness profiling reveals local variations across the WM, HAZ, and BM. The HAZ is particularly important because non-uniform thermal cycles can alter its grain structure, phase distribution, hardness, and mechanical behaviour [16, 17].

Microstructural analysis identifies phase and grain changes across the WM, HAZ, and BM, helping explain the effects of preheating on hardness and mechanical properties [18, 19, 20].

This study investigates the effect of preheating temperature on the mechanical and microstructural properties of SMAW-welded ASTM A36 steel. Tensile testing, Vickers hardness measurements, and metallographic observations of the WM, HAZ, and BM were used to identify the preheating condition that provides the best balance between mechanical performance and microstructural stability.

2 Materials and methods

2.1 Materials and chemical composition

The base material was 10 mm-thick ASTM A36 steel. S235JR is mentioned only as a broadly comparable EN structural-steel grade, not as a directly equivalent designation. Chemical composition analysis was conducted using optical emission spectroscopy (OES) to determine the main alloying elements in the ASTM A36 steel plate. The measured chemical composition is presented in Table 1.

Table 1. Chemical composition of ASTM A36 steel measured by OES

Element	C	Mn	Si	Cu	P	S
Composition (wt.%)	0.100	0.840	0.250	0.011	0.022	0.006

These results indicate a low-carbon steel composition, which is generally favourable for weldability.

2.2 Preheating procedure

The preheating control system is shown in Fig. 1. A solid-state relay and K-type thermocouple were used to control and monitor the heating temperature during welding. Preheating was treated as an experimental variable rather than determined using a CET-based equation. The non-preheated condition served as the reference, whereas 150 °C, 250 °C, and 350 °C represented low, intermediate, and high preheating levels, respectively. This range was selected to evaluate the effects of controlled cooling and increased thermal input on the mechanical properties, hardness, and microstructure of the welded joint [6, 8, 10, 21].

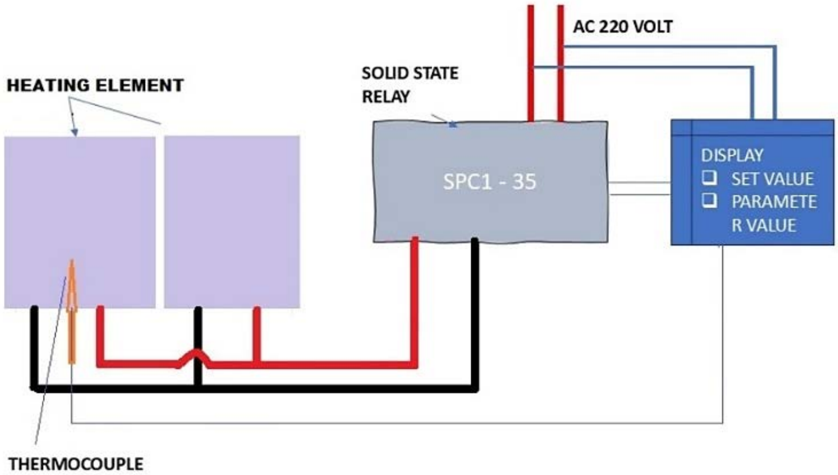

Fig. 1. Schematic diagram of the preheating temperature control system

2.3 SMAW welding procedure

ASTM A36 plates (150 × 300 × 10 mm) were welded using constant WPS parameters; only preheating temperature was varied. The joints were welded in the 1G (PA) flat position using a single V-groove butt-joint configuration in accordance with AWS D1.1/D1.1M [22], with reference to EN ISO 15614-1 and EN ISO 5817 where applicable. The joint geometry consisted of a 60° groove angle, a 2 mm root face, and a 2 mm root opening.

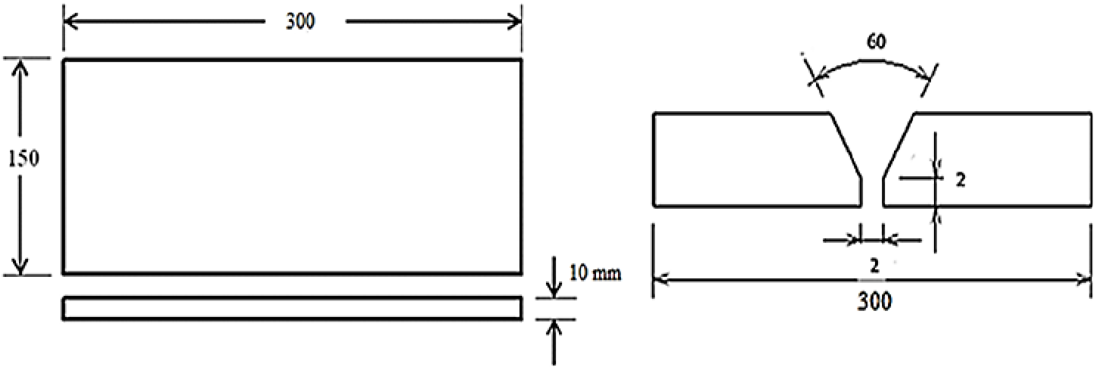

Fig. 2. Dimensions of the welding specimen and bevel joint configuration

The welding process was carried out using the SMAW method under constant-current (CC) conditions. An AWS A5.1 E7016 electrode (Ø 2.6 mm), with reference to EN ISO 2560-A: E 42 4B 12 H5 according to the manufacturer's specification, was utilised for the root pass, whereas AWS A5.1 E7018 (Ø 3.2 mm), with reference to EN ISO 2560-A: E 42 3B 42 H5 according to the manufacturer's specification, was employed for the filler and cap passes.

Fig. 3. Shielded metal arc welding (SMAW) process

Upon completion of welding, all joints were inspected using liquid penetrant testing as part of Non-Destructive Testing (NDT) to identify potential surface defects before further evaluation. The Welding Procedure Specification (WPS), including welding current, arc voltage, travel speed, and calculated heat input, is summarised in Table 2.

Table 2. Welding parameters

Variable	Record
Code / standard acceptance criteria	AWS D1.1, with reference to EN ISO 15614-1 and EN ISO 5817 where applicable
Welding process	SMAW (Shielded Metal Arc Welding)
Polarity	DCEN → Root Pass; DCEP → Fill and Cap Pass
Joint design	Single V-Groove
Material specification	ASTM A36, comparable to S235JR structural steel according to EN 10025-2
Thickness	10 mm
Welding position	1G (Flat Position) according to ISO 6947
Electrode for root pass	AWS A5.1 E7016 Ø 2.6 mm, with reference to EN ISO 2560-A: E 42 4B 12 H5 according to the manufacturer's specification
Electrode for fill and cap pass	AWS A5.1 E7018 Ø 3.2 mm, with reference to EN ISO 2560-A: E 42 3B 42 H5 according to the manufacturer's specification
Welding current	90 A
Arc voltage	24 V
Travel speed	83.91 mm/min
Welding efficiency	0.8
Calculated heat input	1.24 kJ/mm
Inspection	Non-Destructive Testing (NDT), liquid penetrant testing, with reference to EN ISO 3452-1 where applicable

Heat input was calculated using the following equation:

$$HI = \frac{\eta \times V \ x \ I \times 60}{S \times 1000} \quad (1)$$

Where HI is the heat input (kJ/mm), η is the welding process efficiency, V is the arc voltage (V), I is the welding current (A), and S is the travel speed (mm/min). Based on a welding current of 90 A, arc voltage of 24 V, travel speed of 83.91 mm/min, and SMAW efficiency of 0.8, the calculated heat input was 1.24 kJ/mm. The heat input value was included because it directly affects the cooling rate, heat-affected zone (HAZ) characteristics, hardness distribution, and microstructural transformation of SMAW-welded ASTM A36 steel.

2.4 Tensile testing

Tensile testing was performed according to ASTM E8/E8M with reference to EN ISO 6892-1 where applicable, using a 100 kN universal testing machine (UTM) at a constant crosshead speed of 1 mm/min until fracture. Yield strength (YS), ultimate tensile strength (UTS), and elongation were recorded from the tensile test data. Three specimens were tested for each preheating condition, and the results are presented as mean ± standard deviation to evaluate the variability and repeatability of the tensile test results.

Fig. 4. Tensile testing machine

2.5 Hardness testing

Vickers microhardness measurements were performed in accordance with ASTM E92 with reference to EN ISO 6507-1 where applicable, across the BM, HAZ, and WM regions. Indentations were made along a horizontal line across the weld cross-section using a load of 300 gf (0.3 kgf, approximately 2.94 N), a dwell time of 15 s, and a distance of 0.5 mm between adjacent indentation points to prevent overlapping deformation zones.

Fig. 5. Vickers hardness testing machine

2.6 Metallographic preparation and microstructural analysis

Microstructures of the BM, HAZ, and WM were examined following ASTM E407 and, where applicable, EN ISO 17639.. Specimens were ground, polished with 1 µm alumina, etched with 2–5% Nital, and observed by optical microscopy. Calibrated ImageJ grayscale thresholding was used to estimate ferrite, pearlite, and grain size semi-quantitatively.

Fig. 6. Metallographic testing machine and metallographic polishing machine

3 Results and discussion

3.1 Non-destructive testing (NDT)

Fig. 7. Visual and liquid-penetrant inspection results of SMAW-welded joints under no-preheating, 150 °C, 250 °C, and 350 °C conditions

As shown in Fig. 7, all SMAW joints met visual acceptance criteria without major surface defects. The N/A joint showed minor bead irregularities, while 150 °C improved bead uniformity. The 250 °C condition produced the most uniform bead geometry and reinforcement, whereas 350 °C caused slight bead widening due to heat accumulation.

3.2 Tensile testing

Tensile testing determined UTS, YS, and elongation under different preheating conditions. Results are reported as mean ± standard deviation from three specimens. UTS was relatively stable, whereas YS was more sensitive to preheating. All specimens fractured in the BM rather than the WM or HAZ, indicating adequate weld integrity. Fractographic analysis was not performed.

Fig. 8. Post-fracture tensile specimens under different preheating conditions

The fracture locations were identified in the base metal region through macro-observation.

Table 3. Tensile test results of SMAW-welded ASTM A36 steel at different preheating conditions.

Preheating condition	UTS (MPa)	YS (MPa)	Elongation (%)
N/A	446.13 ± 3.82	301.68 ± 5.06	23 ± 1
150 °C	443.42 ± 2.10	307.87 ± 5.32	27 ± 0
250 °C	444.87 ± 1.03	315.68 ± 11.05	23 ± 1

Preheating condition	UTS (MPa)	YS (MPa)	Elongation (%)
350 °C	446.34 ± 1.50	298.70 ± 5.62	24 ± 0

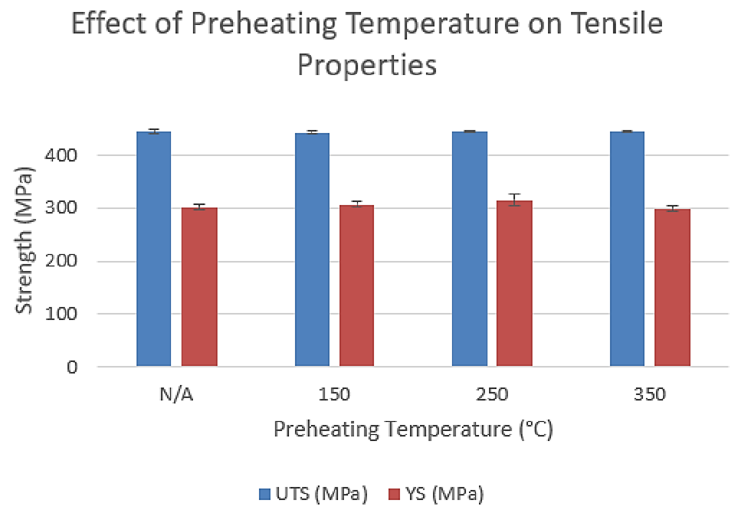

Fig. 9. Tensile properties (UTS and YS) vs. preheating temperature (mean ± SD)

Figure 9 shows the tensile properties of welded joints at different preheating temperatures, reported as mean ± standard deviation ((n=3)). The non-preheated joint exhibited a UTS of (446.13 \pm 3.82) MPa and a YS of (301.68 \pm 5.06) MPa, which served as the baseline condition. The higher thermal gradients and faster cooling without preheating may influence phase evolution and tensile behaviour in welded carbon steel [20]. Preheating at 150 °C slightly decreased the UTS to 443.42 ± 2.10 MPa but increased the YS to 307.87 ± 5.32 MPa, suggesting moderated thermal conditions during welding. Preheating can modify the temperature distribution and residual-stress development in welded components [23], while its influence on the mechanical response of SMAW joints has also been reported for other steels [11, 24]. The 250 °C condition produced the highest YS of 315.68 ± 11.05 MPa with a stable UTS of 444.87 ± 1.03 MPa, reflecting improved microstructural uniformity in the HAZ. Conversely, the 350 °C condition resulted in a comparable UTS of 446.34 ± 1.50 MPa but a lower YS of 298.70 ± 5.62 MPa, indicating possible thermal softening effects. Overall, UTS remained relatively stable within the range of 443–446 MPa, whereas YS was more sensitive to preheating temperature. Therefore, preheating at 250 °C provided the most favourable tensile response among the conditions investigated.

3.3 Hardness testing

Hardness testing was conducted to assess the influence of preheating on SMAW-welded ASTM A36 steel. Vickers hardness (HV) values were evaluated across three distinct regions: Base Metal (BM), Heat-Affected Zone (HAZ), and Weld Metal (WM). The average hardness results for each zone are shown in Fig. 10.

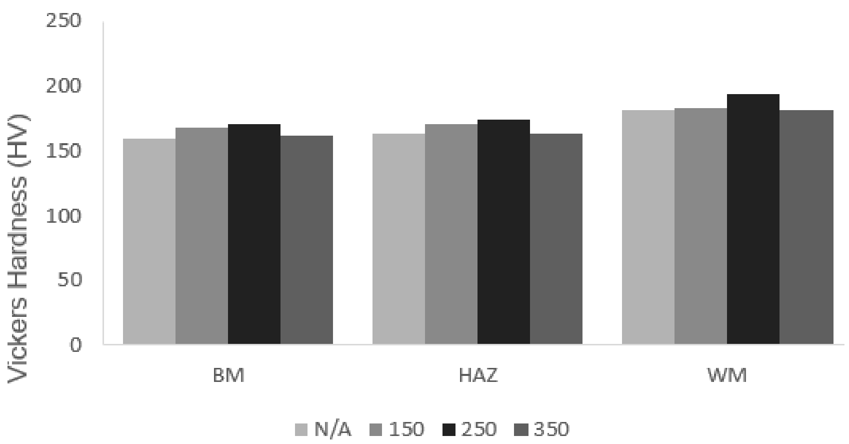

Fig. 10. Average Vickers hardness values in the BM, HAZ, and WM regions at different preheating temperatures

The Vickers hardness distribution of SMAW-welded ASTM A36 joints under N/A, 150, 250, and 350 °C preheating conditions was evaluated across the WM, HAZ, and BM regions. The WM showed the highest hardness (195–210 HV), which may be associated with deposited-metal composition and solidification microstructure. In SMAW joints, local hardness variations are influenced by weld-metal microstructure, heat input, and the local thermal cycle across the WM, HAZ, and BM [25, 26]. The HAZ exhibited lower and more variable hardness in the non-preheated and 150 °C conditions, indicating a less uniform thermal cycle in the present joints. The absence or variation of preheating can modify temperature gradients, cooling history, and phase development in welded steel [20, 27]. Preheating at 250 °C produced the most uniform WM–BM hardness transition, suggesting a balanced cooling condition and microstructural development [28]. In contrast, 350 °C reduced HAZ hardness, suggesting thermal softening and grain coarsening. BM hardness remained stable (155–170 HV), while preheating mainly affected the HAZ. The 250 °C condition produced the most uniform hardness profile and higher yield strength.

3.4 Microstructural analysis

3.4.1 Microstructure of the non-preheated welded joint

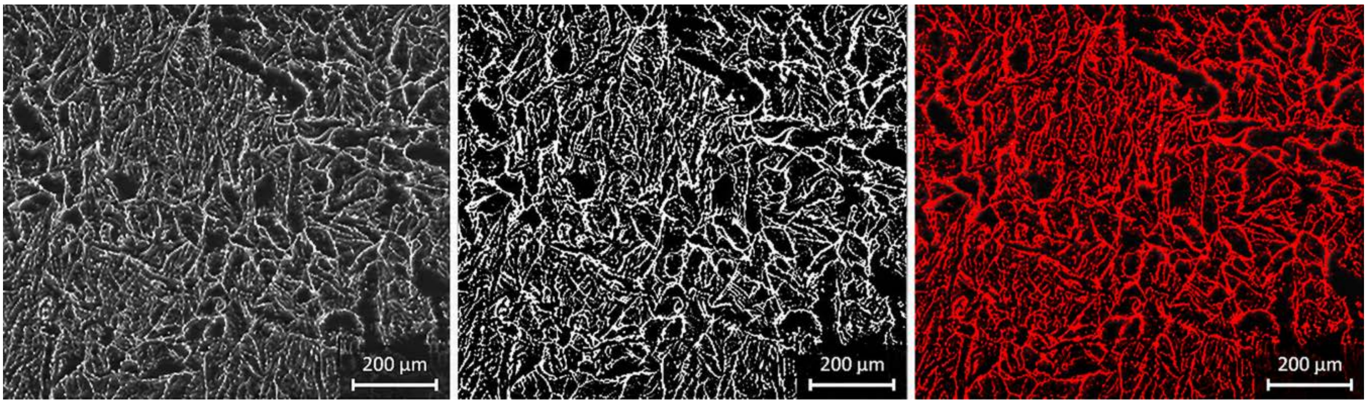

a) b) c)

Fig. 11. Optical micrograph of the weld metal region without preheating: a) grayscale b) threshold c) overlay

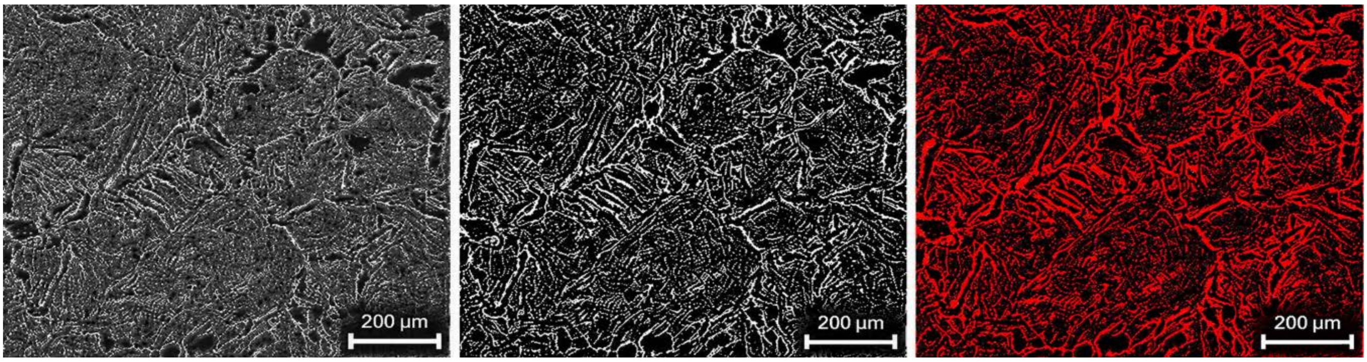

a) b) c)

Fig. 12. Optical micrograph of the heat-affected zone without preheating: a) grayscale b) threshold c) overlay

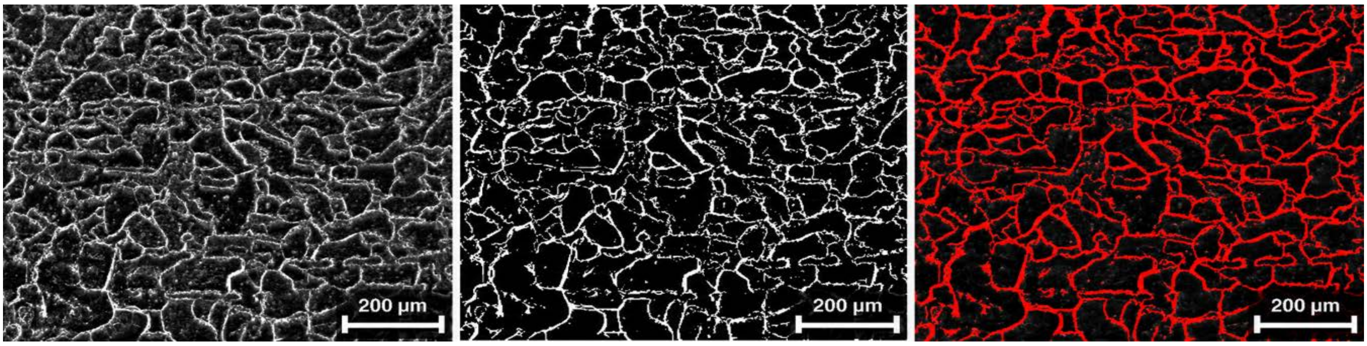

a) b) c)

Fig. 13. Optical micrograph of the base metal region without preheating: a) grayscale b) threshold c) overlay

3.4.2 Microstructure of the welded joint preheated at 150 °C

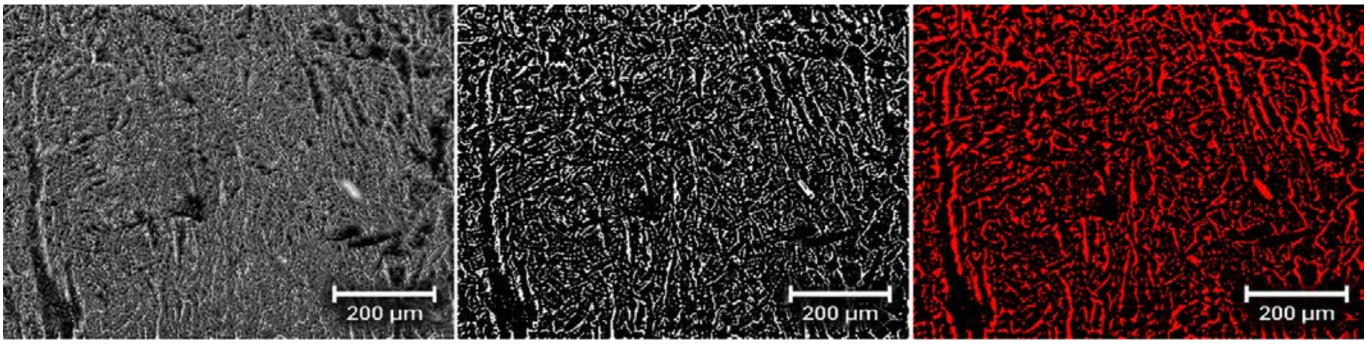

a) b) c)

Fig. 14. Optical micrograph of the weld metal region preheated at 150 °C: a) grayscale b) threshold c) overlay

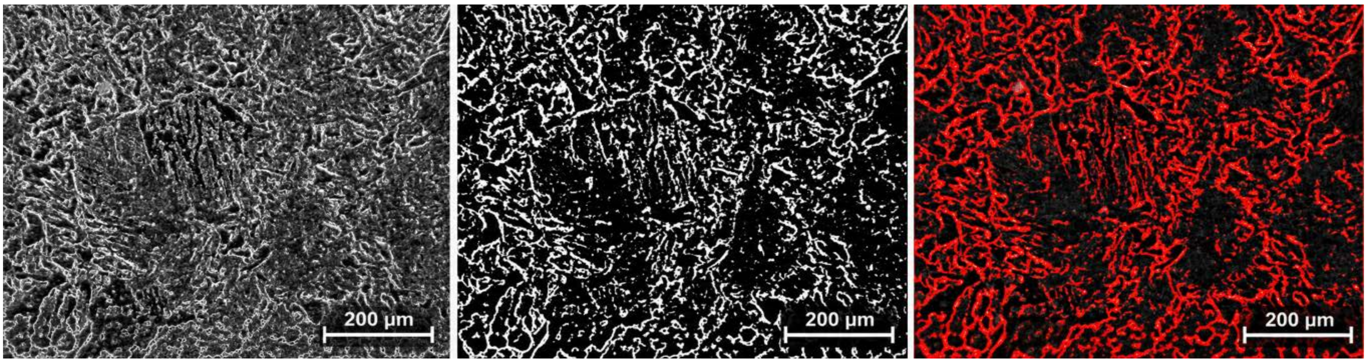

a) b) c)

Fig. 15. Optical micrograph of the heat-affected zone preheated at 150 °C: a) grayscale b) threshold c) overlay

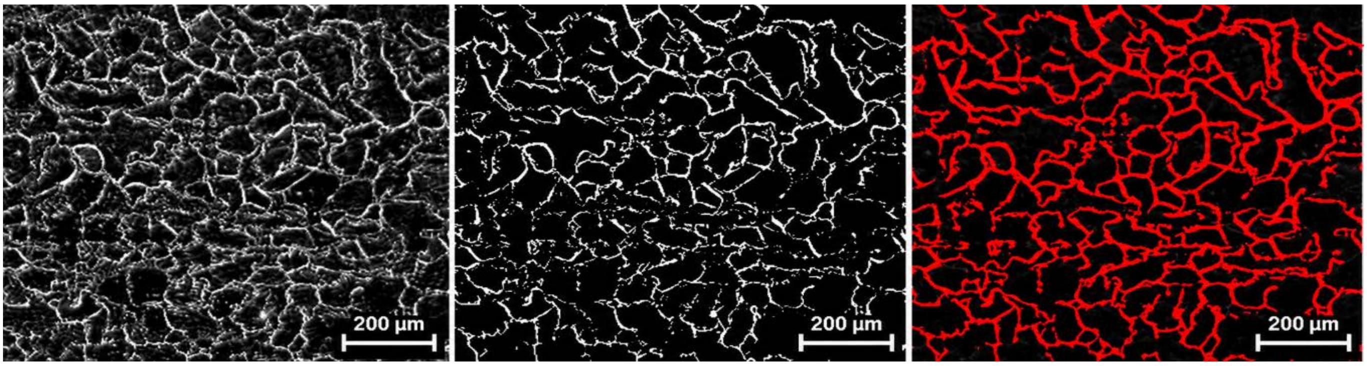

a) b) c)

Fig. 16. Optical micrograph of the base metal region preheated at 150 °C: a) grayscale b) threshold c) overlay

3.4.3 Microstructure of the welded joint preheated at 250 °C

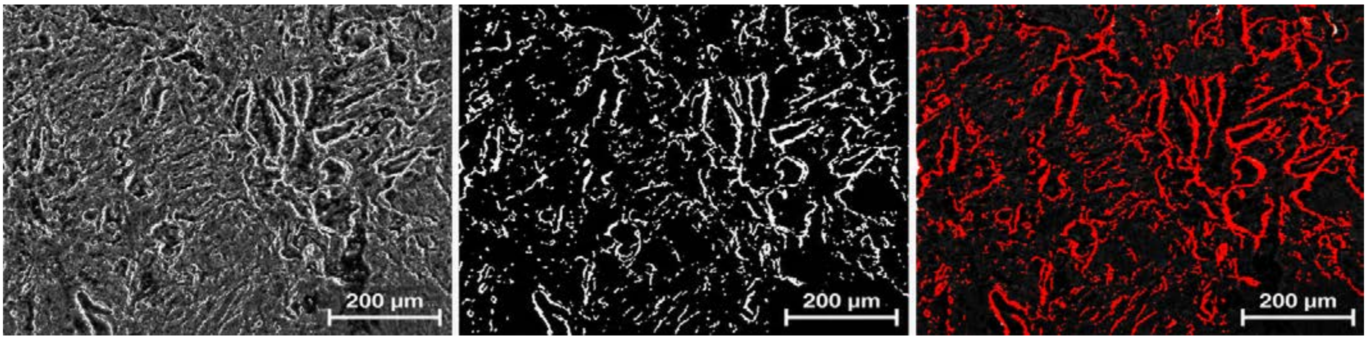

a) b) c)

Fig. 17. Optical micrograph of the weld metal region preheated at 250 °C: a) grayscale b) threshold c) overlay

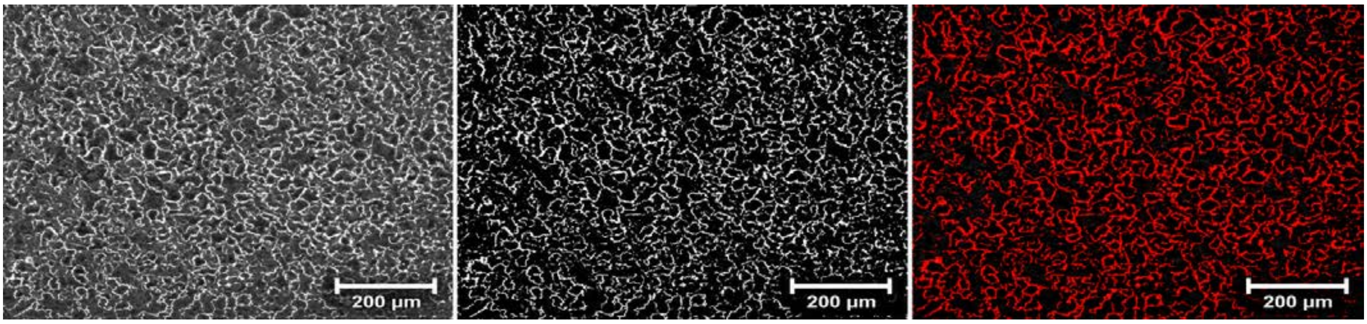

a) b) c)

Fig. 18. Optical micrograph of the heat-affected zone preheated at 250 °C: a) grayscale b) threshold c) overlay

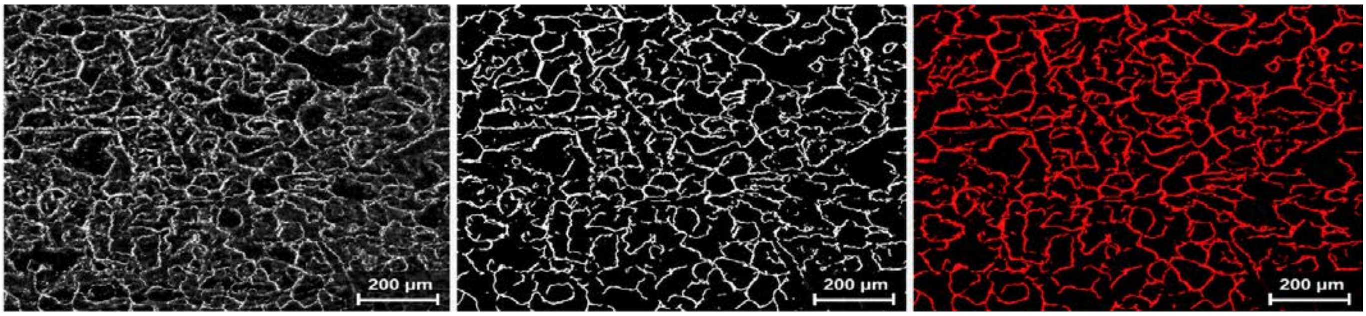

a) b) c)

Fig. 19. Optical micrograph of the base metal region preheated at 250 °C: a) grayscale b) threshold c) overlay

3.4.4 Microstructure of the welded joint preheated at 350 °C

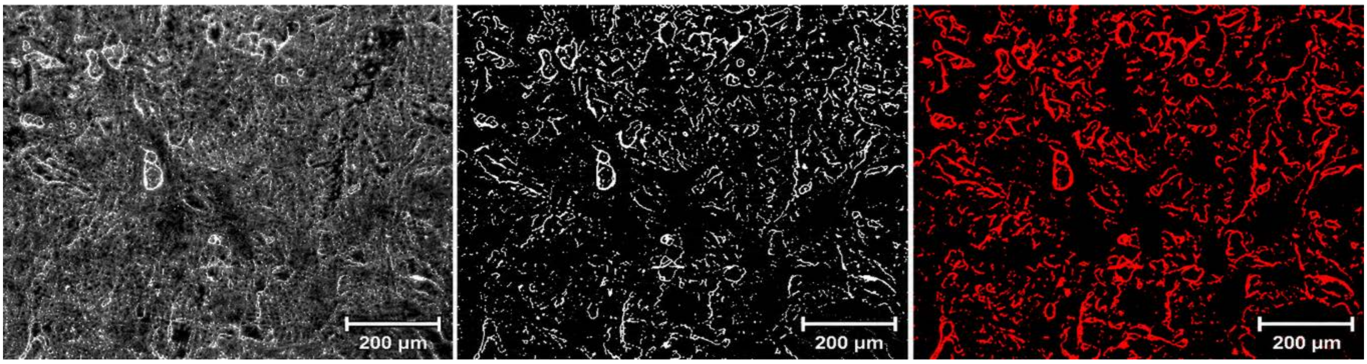

a) b) c)

Fig. 20. Optical micrograph of the weld metal region preheated at 350 °C: a) grayscale b) threshold c) overlay

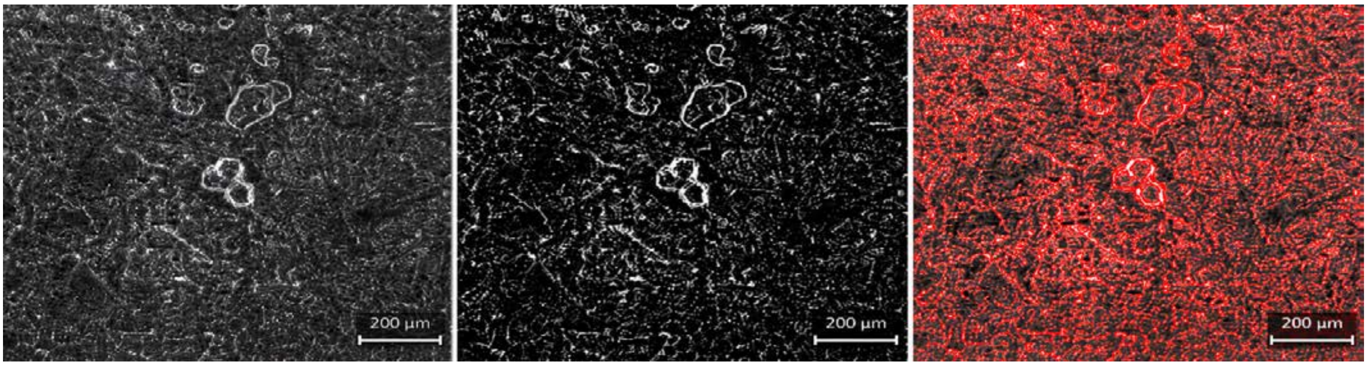

a) b) c)

Fig. 21. Optical micrograph of the heat-affected zone preheated at 350 °C : a) grayscale b) threshold c) overlay

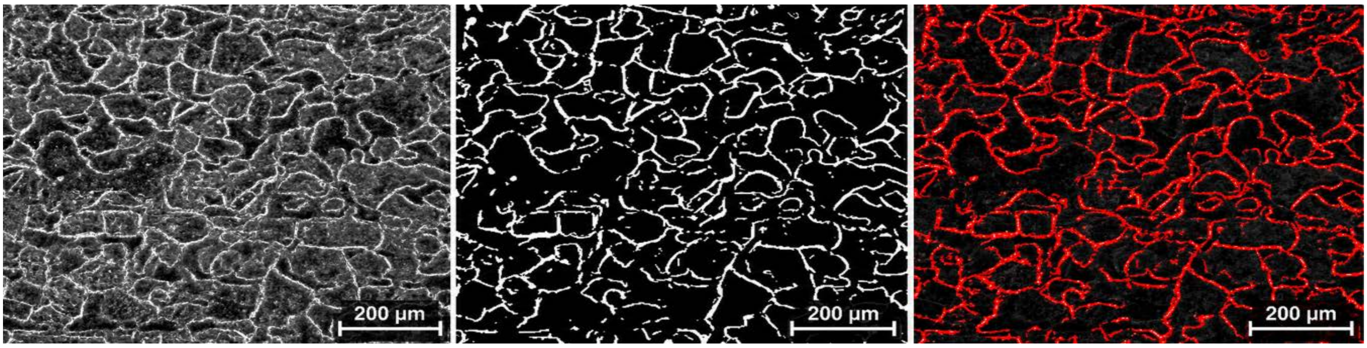

a) b) c)

Fig. 22. Optical micrograph of the base metal region preheated at 350 °C: a) grayscale b) threshold c) overlay

Ferrite and pearlite contents in Table 4 were estimated by semi-quantitative ImageJ segmentation of calibrated grayscale micrographs. Thresholding identified ferrite as bright and pearlite as dark, with ranges representing the minimum–maximum area fractions in the WM, HAZ, and BM.

Table 4. Semi-quantitative microstructural segmentation of ASTM A36 steel under different preheating conditions

Preheating Condition	Zone	Ferrite (%)	Pearlite (%)	Morphology	Characteristics
N/A	WM	70–76	24–30	Fine acicular + partially columnar	Refined solidification structure; ferrite-dominant matrix with dispersed pearlite; compact but less thermally stabilised
	HAZ	64–72	28–36	Coarse equiaxed + partially transformed	Transitional microstructure with localised grain coarsening due to steep thermal gradient
	BM	78–85	15–22	Equiaxed ferrite–pearlite	Stable base metal structure; unaffected by welding heat
150 °C	WM	72–78	22–28	Fine acicular + refined equiaxed	Improved phase uniformity; reduced thermal shock; moderate grain refinement
	HAZ	66–73	27–34	Coarse equiaxed + partially transformed	Controlled grain growth; more homogeneous ferrite–pearlite distribution
	BM	77–84	16–23	Equiaxed ferrite–pearlite	Stable and uniform microstructure
250 °C	WM	74–80	20–26	Refined acicular + equiaxed	Most homogeneous solidification structure; balanced ferrite–pearlite distribution; optimal condition
	HAZ	69–76	24–31	Medium equiaxed + partially transformed	Improved microstructural stability; moderate grain growth
	BM	78–85	15–22	Equiaxed ferrite–pearlite	Stable base metal; negligible structural alteration
350 °C	WM	70–76	24–30	Moderately coarse acicular + partial columnar	Grain coarsening due to excessive thermal input; reduced refinement
	HAZ	63–71	29–37	Coarse equiaxed + partially transformed	Pronounced grain growth; heterogeneous ferrite–pearlite distribution
	BM	77–84	16–23	Equiaxed ferrite–pearlite	Stable microstructure with slight grain enlargement

Metallographic observations, supported by image segmentation, indicated that preheating influenced the phase distribution and grain development across the WM, HAZ, and BM. Variations in welding thermal conditions can produce different microstructural features and local hardness levels across these regions in SMAW-welded structural steels [25]. Without preheating, rapid cooling produced fine acicular features in the WM and a heterogeneous HAZ, while the BM retained its ferrite–pearlite structure. Preheating at 150 °C improved microstructural uniformity, whereas 250 °C produced the most homogeneous ferrite–pearlite distribution with controlled grain growth. This trend is consistent with previous findings on preheated arc-welded mild steel joints [12]. At 350 °C, greater thermal exposure promoted HAZ grain coarsening and non-uniform pearlite distribution, consistent with the increased HAZ size and cooling time (t_{8/5}) at higher preheating temperatures [28]. The interpretation is further consistent with reports that increased welding heat input and longer cooling times can promote microstructural coarsening near the melting boundary or within the weld region [29, 30]. Overall, the microstructure showed a refinement–stabilization–coarsening tendency, with 250 °C providing the most favourable microstructural stability.

Preheating improved thermal control and microstructural uniformity, consistent with previous mild-steel welding studies [12]. The 250 °C condition produced the highest yield strength and the most uniform hardness distribution. In contrast, the lower yield strength at 350 °C may be associated with prolonged thermal exposure, slower cooling, and local softening [15, 28, 30]. Therefore, 250 °C provided the most favourable balance of strength, hardness uniformity, and ferrite–pearlite stability.

Although the 150 °C condition showed the highest elongation, the 250 °C condition provided the highest yield strength, a comparable UTS, a comparatively uniform hardness distribution, and a more homogeneous ferrite–pearlite microstructure. Therefore, 250 °C was identified as the most favourable preheating condition based on the combined mechanical and microstructural criteria.

This study is limited to the investigated preheating temperatures of N/A, 150 °C, 250 °C, and 350 °C. Residual stress measurement, impact toughness testing, and SEM-based fracture analysis were not conducted. Future studies should include these analyses and advanced microstructural characterization to provide a more comprehensive understanding of SMAW-welded ASTM A36 steel.

4 Conclusion

This study demonstrates that preheating temperature significantly influences the mechanical and microstructural behaviour of SMAW-welded ASTM A36 steel. While ultimate tensile strength remained relatively stable, yield strength and ductility were temperature dependent. The 250 °C condition provided the highest yield strength and the most uniform hardness distribution, indicating moderated cooling and improved structural stability. Microstructural analysis confirmed a refinement–stabilisation–coarsening progression with increasing preheating temperature, with 250 °C yielding the most homogeneous ferrite–pearlite structure, whereas 350 °C promoted grain coarsening and thermal softening. Therefore, 250 °C is identified as the most favourable preheating temperature within the investigated conditions for achieving a balanced combination of yield strength, ductility, hardness uniformity, and microstructural stability.

5 Acknowledgements

The authors would like to express their sincere gratitude to Diponegoro University for the academic and institutional support provided during the completion of this research.

6 References

[1] Kjell, E., Kaiser, S., Rhode, M., Kannengiesser, T., & Kromm, A. (2025). In-service and repair welding of pressurized hydrogen pipelines: A review on current challenges and strategies. *Welding in the World*, 69(10), 3141–3164. https://doi.org/10.1007/s40194-025-02127-x

[2] Senthilkumar, S., Manivannan, S., Venkatesh, R., & Karthikeyan, M. (2023). Influence of heat input on the mechanical characteristics, corrosion and microstructure of ASTM A36 steel welded by GTAW technique. *Heliyon*, 9(9), e19708. https://doi.org/10.1016/j.heliyon.2023.e19708

[3] Nickabadi, S., Rostami, H., Hadavi, M., & Rostami, E. (2025). Experimental and numerical investigation of the welding impact on residual stresses of the joint region of ASTM-A36 marine steel. *Materials Chemistry and Physics*, 339, 130738. https://doi.org/10.1016/j.matchemphys.2025.130738

[4] Falodun, O., Oke, S., & Bodunrin, M. (2025). A comprehensive review of residual stresses in carbon steel welding: Formation mechanisms, mitigation strategies, and advanced post-weld heat treatment techniques. *The International Journal of Advanced Manufacturing Technology*. https://doi.org/10.1007/s00170-025-15088-8

[5] Preedawiphat, P., Mahayotsanun, N., Sa-ngoen, K., & Noipitak, M. (2020). Mechanical investigations of ASTM A36 welded steels with stainless steel cladding. *Coatings*, 10(9), 844. https://doi.org/10.3390/coatings10090844

[6] Addai, B., Gyimah, K. O., Asumadu, T. K., Anto, M., Klenam, D. E. P., & Soboyejo, W. O. (2024). Strain gradient plasticity in AISI A36 plain carbon steel weldment: Comparison of butt and lap joint configurations. *Results in Engineering*, 22, 102078. https://doi.org/10.1016/j.rineng.2024.102078

[7] Pratiwi, D. K., Arifin, A., & Mardhi, A. (2023). Investigation of welding parameters of dissimilar weld of SS316 and ASTM A36 joint using a grey-based Taguchi optimization approach. *Journal of Manufacturing and Materials Processing,* 7(1), 39. https://doi.org/10.3390/jmmp7010039

[8] Schaupp, T., Schrouder, N., Schroepfer, D., & Kannengiesser, T. (2021). Hydrogen-assisted cracking in GMA welding of high-strength structural steel—A new look into this issue at narrow groove. *Metals*, 11(6), 904. https://doi.org/10.3390/met11060904

[9] Ji, J., Yuan, H., Zhong, Y., Cui, G., Xu, L., & Wang, X. (2023). Effects of different pre-heating welding methods on the temperature field, residual stress and deformation of a Q345C steel butt-welded joint. *Materials*, 16(13), 4782. https://doi.org/10.3390/ma16134782

[10] Xie, L., Shi, W., Wu, T., Gong, M., Cai, D., Han, S., & Kong, H. (2022). Effect of dynamic preheating on the thermal behavior and mechanical properties of laser-welded joints. *Materials*, 15(17), 6159. https://doi.org/10.3390/ma15176159

[11] Arifin, A., Wijaya, M. R. Y. Q. A., Ode, L., Barata, A., & Ramli, M. I. (2024). The effect of preheating on the mechanical properties of AISI 1037 and AISI 304 welded joints using shielded metal arc welding. *Materials*, 17(23), 5780. https://doi.org/10.3390/ma17235780

[12] Shaikh, S., Shajib, S., Kader, A., Mondal, D., & Islam, A. (2025). Effect of preheating on microstructure and mechanical properties in mild steel arc weld joints. *International Journal of Automotive and Mechanical Engineering,* 22(1), 12133–12145. https://doi.org/10.15282/ijame.22.1.2025.14.0931

[13] Wang, L., Li, H., Huang, Y., Wang, K., & Zhou, M. (2022). Effect of preheating on martensitic transformation in the laser beam welded AH36 steel joint: A numerical study. *Metals*, 12(1), 127. https://doi.org/10.3390/met12010127

[14] Alipooramirabad, H., Cornish, N., Kurji, R., Roccisano, A., & Ghomashchi, R. (2023). Quenched and tempered steels welded structures: Modified gas metal arc welding-pulse vs. shielded metal arc welding. *Metals*, 13(5), 887. https://doi.org/10.3390/met13050887

[15] Neumann, M., Hälsig, A., & Hensel, J. (2024). Influence of welding thermal cycles on properties of TMCP and Q&T steels evaluated by thermo-physical simulation. *Welding in the World*, 68, 183–197. https://doi.org/10.1007/s40194-023-01615-2

[16] Dornelas, H. P., Payão, C., Hugo, V., & Moraes, P. (2024). Influence of interpass temperature on the simulated coarse-grained heat-affected zone of a circumferentially welded 2.25Cr-1Mo steel pipe joint. *Journal of Manufacturing and Materials Processing*, 8(6), 248. https://doi.org/10.3390/jmmp8060248

[17] Gonzalez, A. H. R., Bastos, A. E. B., Casadiego, P. L. M., & Niebles, E. E. N. (2023). Influence of heat input on the weldability of ASTM A131 DH36 fillet joints welded by SMAW under wet underwater welding. *Sustainability*, 15(14), 11222. https://doi.org/10.3390/su151411222

[18] Shin, Y., Jung, C., Bae, S., An, G., Son, M., & Park, Y. (2025). Characteristics of microstructure and fracture toughness according to the groove shape of submerged arc welding. *Metals*, 15(1), 10. https://doi.org/10.3390/met15010010

[19] Franceschi, M., Edoardo, B., Alvise, M., Miotti-Bettanini, L., Campagnolo, S., Zambon, L., & Pezzato, M. (2024). Effect of the welding technique and post-welding heat treatments on the microstructure and mechanical properties of a high silicon nanostructured carbide-free bainitic steel. *Journal of Materials Research and Technology*, 31, 718–732. https://doi.org/10.1016/j.jmrt.2024.06.075

[20] Mirza, M. J., Muhammad, A., Hussain, S., Pruncu, C., & Ahmad, W. (2021). Revealing the microstructure and mechanical attributes of pre-heated conditions for gas tungsten arc welded AISI 1045 steel joints. *International Journal of Pressure Vessels and Piping*, 192, 104440. https://doi.org/10.1016/j.ijpvp.2021.104440

[21] Mkanna, L. (2024). A practical-based determination of preheating temperature of high strength steels welding. *Technical and Educational Sciences*, 14(2), 1–14. https://doi.org/10.24368/jates375

[22] American Welding Society. (2025*). Structural welding code—Steel*. American Welding Society.

[23] He, J., Wei, M., Zhang, L., Re, C., Wang, J., Wang, Y., & Qian, W. (2022). Effect of preheat temperature and welding sequence on the temperature distribution and residual stress in the weld overlay repair of hydroturbine runner. *Materials*, 15(14), 4867. https://doi.org/10.3390/ma15144867

[24] Process, S. (n.d.). An integrated approach of GRA coupled with principal component analysis for multi-optimization of shielded metal arc welding.

[25] Kumar, V., Yadav, S. K., Vijetha, K., Mendhe, V., Kumari, A., Shrivastava, V., Goga, G., & Jain, A. (2025). An investigation of the effect of GMAW and SMAW processes on mechanical and microstructural properties of welded E350 grade steel. *Scientific Reports*, 15(1), 36338. https://doi.org/10.1038/s41598-025-20140-4

[26] Pinto, R., Luis, G., Peral, B., Francisco, M., & Belzunce, J. (2025). Influence of heat input and post-weld heat treatment on the properties of the heat affected zone and weld metal of welded joints on S690QL steel. *The International Journal of Advanced Manufacturing Technology*, 4011–4028. https://doi.org/10.1007/s00170-025-16083-9

[27] Andersson, B., Steyn, E., Ekh, M., & Josefson, L. (2025). Simulation-based assessment of railhead repair welding process parameters. *Welding in the World*, 177–197. https://doi.org/10.1007/s40194-024-01837-y

[28] Sun, J., & Dilger, K. (2023). Influence of preheating on residual stresses in ultra-high strength steel welded components. *Journal of Materials Research and Technology*, 25, 3120–3136. https://doi.org/10.1016/j.jmrt.2023.06.181

[29] Doredla, N., & N. S. K. (2025). Determination of heat input impact on residual stress, microstructure and mechanical characteristics of welded ferrite-pearlite (α-P) steel joints by using Taguchi optimization approach. *Journal of Advanced Joining Processes*, 11, 100278. https://doi.org/10.1016/j.jajp.2024.100278

[30] Rust, B., Schmidt, J., & Stroetmann, R. (2025). Influence of the cooling time t8/5 on weld metals. *Welding in the World*, 69(10), 2961–2974. https://doi.org/10.1007/s40194-025-01942-6

7 Conflict of interest statement

The authors declare no conflict of interest.

8 Author contributions

Sumarji Marji: conceptualization and methodology, experimental investigation, data analysis and validation, microstructural characterization, writing – original draft. Agus Hariyanto: conceptualization and methodology, supervision and correspondence, Writing – review and editing. Arif Wahyudiyanto: data analysis and validation, writing – review and editing. Agus Suprihanto: microstructural characterization, writing – review and editing. Wajilan: data analysis and validation, writing – review and editing.

9 Availability statement

All relevant data are included within the article.

10 Supplementary materials

There are no supplementary materials to include.

Paper submitted: 06.03.2026.
Paper accepted: 05.07.2026.